This is the accepted manuscript made available via CHORUS. The article has been published as:

Realizing the Haldane Phase with Bosons in Optical Lattices

Junjun Xu, Qiang Gu, and Erich J. Mueller

Phys. Rev. Lett. **120**, 085301 — Published 23 February 2018

DOI: 10.1103/PhysRevLett.120.085301

Realizing the Haldane phase with bosons in optical lattices

Junjun Xu,[1,2] Qiang Gu,[1,*] and Erich J. Mueller[2,†]

[1] *Department of Physics, University of Science and Technology Beijing, Beijing 100083, China*
[2] *Laboratory of Atomic and Solid State Physics, Cornell University, Ithaca, New York 14853, USA*

(Dated: February 1, 2018)

We analyze an experimentally realizable model of bosons in a zig-zag optical lattice, showing that by rapidly modulating the magnetic field one can tune interaction parameters and realize an analog of the Haldane phase. We explain how quantum gas microscopy can be used to detect this phase's non-local string order and its topological edge states. We model the detection process. We also find that this model can display supersolid correlations, but argue that they only occur at parameter values which would be challenging to realize in an experiment.

In the past 30 years, one of the dominant themes in condensed matter theory has been the search for models where the collective excitations behave unlike any known fundamental particle. While many such fractionalized and topologically ordered models have been found [1], very few of them have been experimentally realized. Here we show how to build on a setup proposed by the NIST cold atom experimental group [2] to explore one of the iconic fractionalized phases, the Haldane phase of a spin-1 chain [3].

In 1983, Haldane showed that the properties of integer and half-integer spin chains can be profoundly different [3, 4]. Over the following decade, several researchers explored the rich properties of the integer spin chain, finding half integer spin edge modes [5–7], and non-local string order [8–10]. More recently, Dalla Torre, Berg, and Altman noted that similar physics should occur for spinless bosons hopping on a one-dimensional lattice: the occupation numbers on each site plays the role of the different spin states [11, 12]. Subsequently, analogs of the Haldane phase have been predicted for a number of one-dimensional Bose-Hubbard models with off-site interactions [13–16]. One enlarges the parameter range over which the Haldane phase is stable if there is a constraint on the maximum number of particles per site. By combining a number of experimental techniques, we show how to realize a model which would be expected to support the Haldane phase. We use Density Matrix Renormalization Group (DMRG) techniques to calculate the properties of this model [17, 18], and explain how to detect the exotic signatures of the Haldane phase.

In a system of one-dimensional lattice bosons, the Haldane (HI) phase lies at the intersection of the density wave (DW) phase, where double occupied sites (doublons) alternate with empty sites (holons), the Mott insulator (MI) phase, where each site is occupied by a single atom, and the superfluid (SF) phase, where the quasiparticles (doublons and holons) are free to move around. In the Haldane phase the quasiparticles are fluid but ordered: their spacing varies, but as one moves from left to right the next quasiparticle after a doublon is a holon, and vice-versa. This ground state is four-fold degenerate in a large but finite system with hard-wall boundary conditions – corresponding to the flavors of the leftmost and rightmost quasiparticles – which are bound to the edges of the system. This four-fold degeneracy was also found in the original spin context, corresponding to two spin-1/2 degrees of freedom, one sitting at each boundary.

One-dimensional bosonic system have been realized by trapping cold atoms in elongated optical traps [19–21]. Anisimovas *et al.* showed that by using a one-dimensional (1D) spin dependent optical lattice and Raman induced hopping, one could produce the zig-zag lattice illustrated in Fig. 1(a), described by the tight-binding model [2]

$$\begin{aligned} H = & t\sum_j (c^\dagger_{1,j}c_{-1,j} + c^\dagger_{1,j-1}c_{-1,j} + \text{H.c.}) \\ & - t'\sum_{j,s}(c^\dagger_{s,j+1}c_{s,j} + c^\dagger_{s,j}c_{s,j+1}) + \frac{U}{2}\sum_{j,s} n_{s,j}(n_{s,j}-1) \\ & + U_2\sum_j [n_{1,j} + n_{1,j-1}]n_{-1,j}. \end{aligned} \tag{1}$$

Here $s = \pm 1$ labels the spin state of the atoms and j is the position of the atom along the lattices. The hopping between and within these two spin states are characterized by t and t'. The on-site and nearest interspecies interaction are described by U and U_2. Following Anisimovas *et al.* and shown in Fig. 1(a), one can think of Eq. (1) in one of two ways: either as a two-leg "zig-zag" lattice, or a 1D chain with next-nearest neighbor hopping. The latter is closer to the actual physical system. Following that interpretation, we introduce operators $b_{2j} = c_{-1,j}$ and $b_{2j+1} = c_{+1,j}$, in which case t, t' are nearest and next-nearest neighbor hopping parameters, while U, U_2 are on-site and nearest neighbor interaction parameters, i.e. $H = t\sum_i (b^\dagger_{i+1}b_i + b^\dagger_i b_{i+1}) - t'\sum_i (b^\dagger_{i+2}b_i + b^\dagger_i b_{i+2}) + \frac{U}{2}\sum_i n_i(n_i-1) + U_2\sum_i n_{i+1}n_i$. Aside from the longer range hopping, Eq. (1) maps onto the model introduced by Dalla Torre *et al.* in considering polar molecules in optical lattices. Unfortunately, based on their analysis, one expects that the Haldane phase is not stable when U/U_2 is large – which is the physically relevant regime considered in [2]. (Our numerics confirm this expectation.) Here we argue that by using a Feshbach resonance [22],

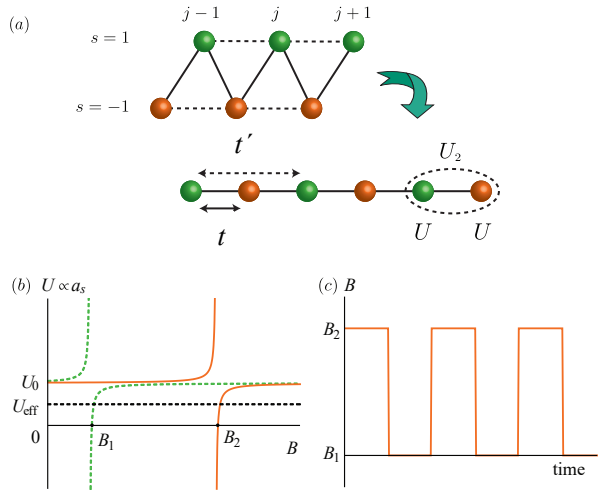

FIG. 1. (Color Online) (a) Schematic of the experimental system, which can be interpreted as a zig-zag ladder or a 1D lattice with next-nearest neighbor hopping. The green and orange colors label two different spin states $s = \pm 1$. (b) On-site interaction U in $F = 1$, $m_F = 0$ (green dashed) and $m_F = 1$ (solid orange) hyperfine states of ^{87}Rb. The background interaction strength U_0 corresponds to the value of U away from the Feshbach resonances near the zero-crossings at B_1 and B_2. Rapidly switching the magnetic field between B_1 and B_2, as illustrated in (c), yields an effective time-averaged on-site interaction $U_{\rm eff} = U_0/2$ in both channels.

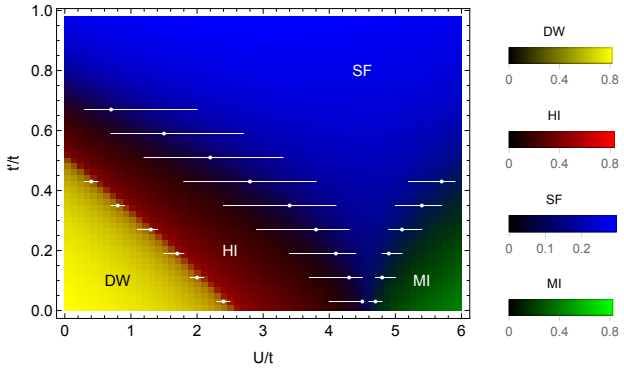

FIG. 2. (Color Online) Representative slice of the phase diagram of the model in Eq. (1). Here $U_2/t = 2.5$, and the maximum occupation of any site is 2. Dots show our best estimate of phase boundaries, as determined by bipartite number fluctuations, and lines represent error bars [27]. Yellow, Red, Blue, and Green show amplitude of the correlation functions in Eq. (2) at a separation of $s = 80$ sites in a chain of length 256. At shorter lengthscales, correlations are of similar size, but the boundaries are less sharp.

one can reduce U, driving the system into the Haldane phase. The lossy nature of bosonic Feshbach resonances aids us, as the quantum Zeno effect converts the resulting large 3-body recombination rate into a suppression of the probability of having more than two particles on any given site – further stabilizing the Haldane phase.

More concretely, we consider the $F = 1$, $m_F = 1, 0$ states of ^{87}Rb. The coefficient U is proportional to the scattering length associated with two atoms in the same magnetic sublevel. As illustrated in Fig. 1(b), this scattering length can be manipulated by applying a magnetic field. Near $B_1 \sim 661.43$G there is a zero-crossing where the interactions between two $m_F = 0$ atoms vanish, while near $B_2 \sim 685.43$G there is a similar zero crossing for $m_F = 1$ [23]. We envision rapidly switching the magnetic field between these two fields, as illustrated in Fig. 1(c). As long as the switching time is short compared to the other scales in the problem ($h/U, h/t \sim h/E_R \approx 0.27$ms for laser wavelength $\lambda = 789$nm) the effective interaction in each spin channel will be given by time-averaging the instantaneous Hamiltonian $U_{\rm eff} = \int_0^t U(\tau)d\tau$ [24–26]. Even though at any given time the interactions in the two channels will be different, this time averaged interaction is the same for each spin species, and U will be the same on all sites. This technique effectively halves the strength of the on-site interaction as in Fig. 1(b). The coefficient U_2 is largely unaffected. We find that one can achieve a ratio of on-site to nearest neighbor interaction of $U/U_2 \approx 1.6$, for a lattice depth of $V_0 = 2E_R$ (for the effect of a higher band, see the Supplemental Material [27]). By appropriately tuning the transverse confinement, one can take $U_2/t = 2.5$, yielding $U/t = 4$. Figure 2 shows the phase diagram for this model, revealing that these parameters place the system within the Haldane phase regime.

The zero crossings are very close to Feshbach resonances, and hence induce a large 3-body loss rate K_3. In the present circumstance this is advantageous. Following the logic in [31], when K_3 is large, there is a strong suppression of the process in which a third particle hops onto a site containing two other particles. This suppression can be modeled by a complex on-site three-body repulsion of strength $U_{3b} \sim -ihK_3n^2/12$. We estimate that one can get $|U_{3b}| \sim 10E_R$ for a typical on-site particle density $n \sim 2.1 \times 10^{15}$cm^{-3} and typical on-resonance three-body rate $K_3 \sim 10^{-25}$cm^6/s. Since $|U_{3b}|$ is larger than the other scales in the problem, it can be replaced by a constraint that no more than two particles can occupy any site.

With this constraint we use the DMRG to calculate the properties of the model in Eq. (1). We start with a infinite DMRG algorithm to grow the system to desired size, and then do finite DMRG sweeps until we reach convergent. This technique is typically understood as systematically optimizing a variational wavefunction in the form of a matrix product state [18]. The degree of approximation is controlled by the bond dimension d. We have considered systems as large as $L = 512$ sites, and bond dimensions as large as $d = 500$. The algorithm is more efficient if we alter the boundary conditions to break the potential four-fold degeneracy of the Haldane-

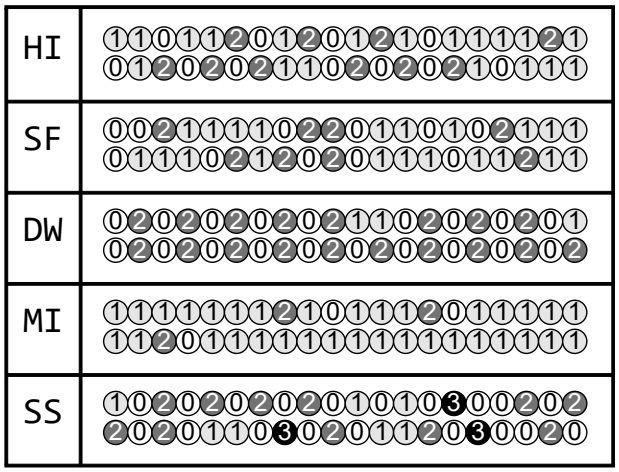

FIG. 3. Typical configurations of occupation numbers extracted from the central 20 sites of our DMRG wavefunctions, modeling single-shot quantum gas microscope images. Configurations correspond to parameters in which different forms of order can be observed: HI($U/t = 4$, $U_2/t = 2.5$ for $t'/t = 0$), SF($U/t = 4$, $U_2/t = 2.5$ for $t'/t = 1$), DW($U/t = 1$, $U_2/t = 2.5$ for $t'/t = 0$), MI($U/t = 10$, $U_2/t = 2.5$ for $t'/t = 0$). The last figure has short-range supersolid correlations: SS($U/t = 0$, $U_2/t = 2.5$ for $t'/t = 0.6$ for maximum occupation number 3). Each circle resembles a single site, and the number in the circle tells how many atoms are on this site. We show two independent realizations for each phase.

phase groundstate, and the potential two-fold degeneracy of the density wave groundstate. In particular we used boundary conditions which pin a vacancy at the left-most site, and doublon at the right-most site. We analyze convergence with bond dimension and system size in the supplementary information. From these studies we expect that experiments on systems of size $L \sim 60$ will see significant finite-size effects near the phase boundaries, but the bulk physics is unchanged, and such experiments will be able to unambiguously observe all of the relevant physical phenomena.

The order in the Haldane, Mott insulator, density wave phases are encoded in string (str), parity (MI) and density wave (DW) correlation functions [8, 12]

$$\begin{aligned} C_{ij}^{\mathrm{str}} &= \left\langle \delta n_i e^{i\pi \sum_{i<k<j} \delta n_k} \delta n_j \right\rangle, \\ C_{ij}^{\mathrm{MI}} &= \left\langle e^{i\pi \sum_{i\le k\le j} \delta n_k} \right\rangle, \\ C_{ij}^{\mathrm{DW}} &= (-1)^{j-i} \left\langle \delta n_i \delta n_j \right\rangle, \end{aligned} \tag{2}$$

where $\delta n_k = n_k - 1$. The phase factor $e^{i\pi \sum_{i<k<j} \delta n_k} = \pm 1$ depends on if the number of quasiparticles between sites i and j is even or odd. In the superfluid phase all of the three correlation functions fall to zero as i and j are separated. In the Haldane/Mott insulator phase, only $C^{\mathrm{str}}/C^{\mathrm{MI}}$ has long-range order, while in the density wave phase all the three correlation functions are nonzero.

We additionally study the single particle density matrix $C_{ij}^{\mathrm{SF}} = \langle b_i^\dagger b_j \rangle$ and the bipartite number fluctuations, $D_j = \langle N_{i<j}^2 \rangle - \langle N_{i<j} \rangle^2$, where $N_{i<j} = \sum_{i=1}^{j-1} n_i$ is the number of particles to the left of site j. The superfluid phase is characterized by power-law behavior of the density matrix, and enhance bipartite number fluctuations when compared to the incompressible insulating phases. We found that these number fluctuations were the most reliable way to extract the phase boundaries between the superfluid and insulating phases [27]. In particular, due to the different scaling with system size, the number fluctuations in half the chain, $D_{L/2}$, form plateaus in each of the phases, and the phase boundaries correspond to peaks in the slope $dD_{L/2}/dt'$. We use the full width half max of these peaks as an estimate of the accuracy of these boundaries. This approach is adapted from [32], and is similar to finding phase boundaries from peaks in specific heat.

Additionally, the DW to HI transition can be accurately determined from the properties of C^{DW}. Applying finite size scaling [33] to the asymptotic behavior of this correlation function yields a DW-HI boundary which agrees with our calculation using the number fluctuations. The various superfluid-insulator transitions are not amenable to this standard finite size scaling analysis: they have behavior related to Kosterlitz-Thouless transitions, and are harder to determine. In addition to our technique of looking at number fluctuations, these transitions can be identified by looking at the excitations spectrum [13] or superfluid stiffness [34], by taking moments of C^{SF} [35, 36], or by comparing the power law decay of C^{SF} to a Luttinger liquid model [37, 38]. More discussion of the critical behavior can be found in [39]. Due to the significant finite size effects, it is unlikely that an experiment would be able to accurately determine these phase boundaries.

The correlation functions in Eq. (2) are directly measurable via a quantum gas microscope [40–44]. One projects the quantum state into one in which there is a definite number of particles on each site – giving a single realization of $\{n_i\}$. Repeating the measurement many times allows one to extract the expectation values in Eq. (2). This technique has already been used to measure the parity order [44].

In addition to showing the phase boundaries, Fig. 2 shows the size of correlations on a length-scale of 80 sites. In a significant part of the phase diagram, the string correlations are large but all other correlation functions vanish. This corresponds to the desired Haldane phase. The HI, DW, and MI correlations at shorter lengths scales are of similar strength, but display less sharp boundaries. As would be expected, the SF correlations are strongly length-dependent. They are also extremely hard to measure in an experiment. The simplest experimental knob for moving through this phase diagram is the strength

of the Raman beams, which changes t while leaving all other scales unchanged. Additionally, both t and t' are exponentially sensitive to the lattice depth, while the ratio between U and U_2 is controlled by modifying the time dependence of the magnetic field.

In addition to exploring the expectation values of the various correlation functions, we use a novel Monte-Carlo sampling algorithm to stochastically generate 'typical' cold-gas microscope images [27]. Given the DMRG wavefunction $|\psi\rangle$, we first calculate the probability that site-1 had $0, 1$ or 2 particles on it. We use these probabilities to choose one of these sectors, and project the wavefunction into that sector. This calculation is then repeated on site-2, using the new wavefunction... Figure 3 shows configurations generated by this algorithm, which should be representative of what is seen in an experiment. We emphasize that these are not cartoons, but rather are unbiased samples. As expected, in the HI phase the doublons and holons alternate, with a variable number of singly-occupied sites between them. This can be contrasted with the SF phase, where there is no ordering of the doublons and holons. In the DW phase, doublons and holons alternate. In these images one sees a small number of defects in the order – as should be expected. In the MI phase the images show very few holons and doublons – and those which exist are tightly bound together. In this figure we also show images with supersolid (SS) correlations that can appear when we relax the constraint forbidding double occupancy. The physics of this regime will be discussed below.

To illustrate the role of the three-body constraint, we repeated our calculations, allowing the on-site particle number to be as large as 3. Figure 4 shows the analog of Fig. 2. All correlations, except those corresponding to SF order, are much weaker. Short and medium range HI, MI, and DW correlations are detectable, but our scaling analysis suggest that for these parameters there is no long-range DW or HI order.

For small on-site interaction U and finite next nearest hopping t', we find a superfluid region with short-range density wave order, which is suggestive of proximity to a supersolid phase (SS). Such a phase would be more familiar in the language of the "zig-zag" ladder picture: The atoms form a superfluid which preferentially sits on one leg of the ladder. An alternative cartoon can be constructed from the DW state "2020202020." Because of the next-nearest neighbor hopping, one can produce a triplon-singlon pair "2020103020," and these defects may be mobile. Forbidding triple occupancy eliminates these excitations, and prevents the occurrence of this phase in the constrained model. In addition to such triplons and singlons, the configurations in Fig. 3 display defects where atoms have hopped from even to odd sublattices. These defects are responsible for the short-range nature of the correlations.

To summarize, we have proposed a way to realize the

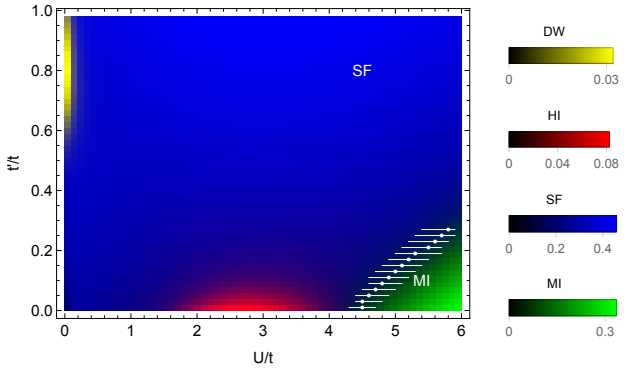

FIG. 4. (Color Online) Representative slice of phase diagram when maximum occupation of any site is 3. All parameters and symbols same as Fig. 2. Note change of scale on color bars. For these parameters there are regions with short or intermediate-range density wave (yellow) or Haldane order (red), but no long-range order.

Haldane phase in a gas of ^{87}Rb atoms trapped in a zigzag optical lattice, where a different atomic spin state is trapped on each leg of the ladder. One reduces the on-site interactions (relative to the nearest neighbor interactions) by rapidly sweeping the magnetic field between two zero-crossings associated with Feshbach resonances in each of the spin states. The proximity to the Feshbach resonances introduces large three-body loss, which via the quantum Zeno effect prevents triple-occupation. We calculate the phase diagram of this model, and find that the Haldane phase is experimentally realizable. We modeled a quantum-gas microscope experiment, and found that one can readily identify the string order of the Haldane phase in individual images. More quantitative tests require averaging over several images. Such averaging has been used to identify other non-local order parameters [44]. We further show that without the constraint on particle number, this model shows hints of a supersolid phase (cf. [45, 46]). One would need to use other techniques, however, to experimentally reach this supersolid regime. Seeing the string order in the Haldane phase would be a remarkable triumph in engineering quantum matter.

J.X. acknowledges helps from Matthew Reichl on the numerical calculation. In addition to our custom-built DMRG software, we performed many of the calculation using the ITensor library (http://itensor.org). E.J.M. acknowledges help from Joshua Squires on aspects related to the phase boundaries. This research is supported by the NBRPC (No. 2013CB922002), NNSFC (No. 11504021, 11574028), NSF (No. PHY-1508300), and FRFCU (No. FRF-TP-17-023A2).

* qgu@ustb.edu.cn
† em256@cornell.edu

[1] C. Chiu, J. C. Y. Teo, A. P. Schnyder, and S. Ryu, Rev. Mod. Phys. **88**, 035005 (2016).
[2] E. Anisimovas, M. Račiūnas, C. Sträter, A. Eckardt, I. B. Spielman, and G. Juzeliūnas, Phys. Rev. A **94**, 063632 (2016).
[3] F. D. M. Haldane, Phys. Lett. A **93**, 464 (1983); Phys. Rev. Lett. **50**, 1153 (1983).
[4] I. Affleck, J. Phys.: Condens. Matter **1**, 3047 (1989).
[5] I. Affleck, T. Kennedy, E. H. Lieb, and H. Tasaki, Phys. Rev. Lett. **59**, 799 (1987); Commun. Math. Phys. **115**, 477 (1988).
[6] M. Hagiwara, K. Katsumata, I. Affleck, B. I. Halperin, and J. P. Renard, Phys. Rev. Lett. **65**, 3181 (1990).
[7] S. H. Glarum, S. Geschwind, K. M. Lee, M. L. Kaplan, and J. Michel, Phys. Rev. Lett. **67**, 1614 (1991).
[8] M. den Nijs and K. Rommelse, Phys. Rev. B **40**, 4709 (1989).
[9] S. M. Girvin and D. P. Arovas, Phys. Scr. **T27**, 156 (1989).
[10] T. Kennedy and H. Tasaki, Phys. Rev. B **45**, 304 (1992); Commun. Math. Phys. **147**, 431 (1992).
[11] E. G. Dalla Torre, E. Berg, and E. Altman, Phys. Rev. Lett. **97**, 260401 (2006).
[12] E. Berg, E. G. Dalla Torre, T. Giamarchi, and E. Altman, Phys. Rev. B **77**, 245119 (2008).
[13] D. Rossini and R. Fazio, New J. Phys. **14**, 065012 (2012).
[14] G. G. Batrouni, R. T. Scalettar, V. G. Rousseau, and B. Grémaud, Phys. Rev. Lett. **110**, 265303 (2013).
[15] S. Ejima, F. Lange, and H. Fehske, Phys. Rev. Lett. **113**, 020401 (2014).
[16] F. Lange, S. Ejima, and H. Fehske, Phys. Rev. Lett. **118**, 120401 (2017).
[17] S. R. White, Phys. Rev. Lett. **69**, 2863 (1992); Phys. Rev. B **48**, 10345 (1993).
[18] U. Schollwöck, Rev. Mod. Phys. **77**, 259 (2005); Ann. Phys. **326**, 96 (2011).
[19] T. Stöferle, H. Moritz, C. Schori, M. Köhl, and T. Esslinger, Phys. Rev. Lett. **92**, 130403 (2004).
[20] T. Kinoshita, T. Wenger, and D. S. Weiss, Science **305**, 1125 (2004).
[21] I. Bloch, Nat. Phys. **1**, 23 (2005).
[22] C. Chin, R. Grimm, P. Julienne, and E. Tiesinga, Rev. Mod. Phys. **82**, 1225 (2010).
[23] A. Marte, T. Volz, J. Schuster, S. Dürr, G. Rempe, E. G. M. van Kempen, and B. J. Verhaar, Phys. Rev. Lett. **89**, 283202 (2002).
[24] S. Blanes, F. Casas, J. A. Oteo, and J. Ros, Phys. Rep. **470**, 151 (2009).
[25] M. Bukov, L. D'Alessio, and A. Polkovnikov, Adv. Phys. **64**, 139 (2015).
[26] A. Eckardt and E. Anisimovas, New J. Phys. **17**, 093039 (2015).
[27] See the Supplemental Material at [url] for a description of DMRG algorithm, detailed explanation of how configuration are sampled, study of higher band effects, scaling with bond dimension, finite size scaling, and finding phase boundaries, which includes Refs. [28–30].
[28] J. R. Garrison and R. V. Mishmash, `https://github.com/simple-dmrg/simple-dmrg`; `https://github.com/iglpdc/dmrg101`.
[29] W. Xu, M. Olshanii, and M. Rigol, Phys. Rev. A **94**, 031601(R) (2016).
[30] O. Dutta, M. Gajda, P. Hauke, M. Lewenstein, D. Lühmann, B. A. Malomed, T. Sowiński, and J. Zakrzewski, Rep. Prog. Phys. **78**, 066001 (2015).
[31] A. J. Daley, J. M. Taylor, S. Diehl, M. Baranov, and P. Zoller, Phys. Rev. Lett. **102**, 040402 (2009).
[32] H. F. Song, S. Rachel, and K. Le Hur, Phys. Rev. B **82**, 012405 (2010); S. Rachel, N. Laflorencie, H. F. Song, and K. Le Hur, Phys. Rev. Lett. **108**, 116401 (2012).
[33] M. E. Fisher, and M. N. Barber, Phys. Rev. Lett. **28**, 1516 (1972).
[34] P. Olsson and P. Minnhagen, Phys. Scr. **43**, 203 (1991).
[35] R. V. Pai and R. Pandit, Phys. Rev. B **71**, 104508 (2005).
[36] H. H. Roomany and H. W. Wyld, Phys. Rev. D **21**, 3341 (1980).
[37] T. D. Kühner, S. R. White, and H. Monien, Phys. Rev. B **61**, 12474 (2000).
[38] X. Deng, R. Citro, E. Orignac, A. Minguzzi, and L. Santos, Phys. Rev. B **87**, 195101 (2013).
[39] J. M. Kurdestany, R. V. Pai, S. Mukerjee, and R. Pandit, arXiv:1211.5202 (2012); arXiv:1403.2315 (2014).
[40] H. Ott, Rep. Prog. Phys. **79**, 054401 (2016).
[41] W. S. Bakr, J. I. Gillen, A. Peng, S. Fölling, and M. Greiner, Nature **462**, 74 (2009).
[42] W. S. Bakr, A. Peng, M. E. Tai, R. Ma, J. Simon, J. I. Gillen, S. Fölling, L. Pollet, and M. Greiner, Science **329**, 547 (2010).
[43] J. F. Sherson, C. Weitenberg, M. Endres, M. Cheneau, I. Bloch, and S. Kuhr, Nature **467**, 68 (2010).
[44] M. Endres, M. Cheneau, T. Fukuhara, C. Weitenberg, P. Schauβ, C. Gross, L. Mazza, M. C. Bañuls, L. Pollet, I. Bloch, and S. Kuhr, Science **334**, 200 (2011).
[45] J. Léonard, A. Morales, P. Zupancic, T. Esslinger, and T. Donner, Nature **543**, 87 (2017).
[46] J. Li, J. Lee, W. Huang, S. Burchesky, B. Shteynas, F. Çağrı Top, A. O. Jamison, and W. Ketterle, Nature **543**, 91 (2017).